Atmos. Chem. Phys. Discuss., 12, 18029–18066, 2012
www.atmos-chem-phys-discuss.net/12/18029/2012/
doi:10.5194/acpd-12-18029-2012

Atmospheric Chemistry and Physics Discussions

Analysis of global methane changes after the 1991 Pinatubo volcanic eruption

N. Bândă[1,2], M. Krol[3,4,1], M. van Weele[2], T. van Noije[2], and T. Röckmann[1]

[1]Institute for Marine and Atmospheric Research Utrecht, Utrecht University, Utrecht, The Netherlands
[2]Royal Netherlands Meteorological Institute (KNMI), De Bilt, The Netherlands
[3]Meteorology and Air Quality, Wageningen University and Research Center, Wageningen, The Netherlands
[4]Netherlands Institute for Space Research (SRON), Utrecht, The Netherlands

Received: 21 June 2012 – Accepted: 22 June 2012 – Published: 19 July 2012

Correspondence to: N. Bândă (n.l.banda@uu.nl)

Published by Copernicus Publications on behalf of the European Geosciences Union.

Abstract

The global methane growth rate showed large variations after the eruption of Mount Pinatubo in June 1991. Both sources and sinks of tropospheric methane were altered following the eruption, by feedback processes between climate and photo-chemistry. Such processes include Ultra Violet (UV) radiative changes due to the presence of volcanic sulfur dioxide (SO_2) and sulphate aerosols in the stratosphere, and due to stratospheric ozone depletion. Changes in temperature and water vapour in the following years caused changes in the tropospheric chemistry, as well as in natural emissions. We quantify the effects that these processes had on methane concentrations using a one-dimensional chemistry model representative for the global tropospheric column. To infer the changes in UV radiative fluxes, we couple the chemistry model to a radiative transfer model. We find that the overall effect of the eruption on the methane growth rate is dominated by the effect of stratospheric ozone depletion. However, all the other processes are found to have non-negligible effects, and should therefore be taken into account in order to obtain a good estimate of methane concentrations after the eruption. We find that the overall effect was a small initial increase in the methane growth rate after the eruption, then a decrease by about 8 ppb yr^{-1} by mid-1993. When changes in anthropogenic emissions are employed according to emission inventories, an additional decrease of about 5 ppb yr^{-1} in the methane growth rate is obtained between the years 1991 and 1993.

1 Introduction

Methane is the second most abundant anthropogenic greenhouse gas in the atmosphere after CO_2. Its concentration in the atmosphere has increased since preindustrial times by a factor of 2.5 (Dlugokencky et al., 2011). A good understanding of the processes responsible for variations in the methane concentration is needed for making future predictions and developing mitigation strategies. However, the evolution of

the methane concentration in the atmosphere in the past two decades is not fully understood (Montzka et al., 2011a). The growth rate of methane was generally positive and showed a decreasing trend during the 80s and 90s, with year to year fluctuations (Dlugokencky et al., 2003). As shown in Fig. 6b, particularly large fluctuations were observed in the years following the eruption of Mount Pinatubo in 1991 (Dlugokencky et al., 1994, 1996; Bekki and Law, 1997; Butler et al., 2004; Bousquet et al., 2006). After a peak of about 16 ppb yr^{-1} near the time of the eruption, the globally averaged methane growth rate dropped to –2 ppb yr^{-1} in late 1992, remaining negative for the second half of the year 1992 (Dlugokencky et al., 2003). A subsequent recovery of the growth rate to 7 ppb yr^{-1} was observed by the end of 1993.

Changes in the global methane concentration are determined by either changes in methane emissions or by changes in the methane lifetime. Methane is emitted from both natural sources (wetlands, oceans and termites) and anthropogenic sources (agriculture, fossil fuel exploitation, waste treatment and biomass burning). The lifetime of methane in the atmosphere is determined by the reaction of methane with the hydroxyl radical (OH) in the troposphere, by the uptake of methane by soils and by the destruction of methane in the stratosphere. The main sink is, however, the reaction with OH, and the other processes contribute by only 10–15 % to the methane loss (Prather et al., 2001; Spahni et al., 2011). Levels of OH are determined by tropospheric photolysis reactions driven by UV radiation, by water vapour levels, and by non-linear tropospheric chemistry. Because OH reacts with these species, its abundance is sensitive to atmospheric concentrations of methane (CH_4), nitrogen oxides (NO_x), carbon monoxide (CO) and non-methane volatile organic compounds (NMVOC). Montzka et al. (2011b) showed by inversions of methyl chloroform that global tropospheric OH is relatively stable to perturbations, having an interannual variability of 2.3 ± 1.5 % for the period 1998 to 2007. Such a small variability was shown to be consistent with the small interannual variability in methane concentrations. In a previous study, Prinn et al. (2005) found an interannual variability in tropospheric OH of 7 to 9 %.

The eruption of Mount Pinatubo triggered a multitude of photochemical effects (McCormick et al., 1995), including feedbacks between climate and atmospheric photochemistry, which contributed to the observed evolution of the methane concentrations. The different processes had both positive and negative impacts on the methane growth rate, affecting methane emissions and the methane lifetime. From satellite observations it is estimated that the eruption emitted about 18 ± 4 Tg (Guo et al., 2004). Volcanic SO_2 absorbs UV radiation between 290 nm and 330 nm, thus its presence in the stratosphere would lead to a decrease in tropospheric photolysis (Dlugokencky et al., 1996). Since OH formation in the troposphere depends on the photolysis of ozone to $O(^1D)$, the UV absorption by SO_2 would lead to a longer methane lifetime. SO_2 stayed in the stratosphere for a few months, forming sulphate aerosols with an e-folding time of 23–25 days (Guo et al., 2004). Sulphate aerosols have been observed by the SAGE II satellite instrument for up to 4 yr after the eruption at heights between 15 and 30 km with a maximum aerosol optical depth (AOD) at 550 nm of approximately τ = 0.15 about 7 months after the eruption (Russell et al., 1996; Thomason et al., 1997). Scattering of solar radiation by sulphate aerosols would lead to a further reduction of photolysis frequencies in the troposphere, thus to a longer methane lifetime. Another secondary effect on the methane lifetime is triggered by the destruction of stratospheric ozone on sulphate aerosols. A maximum global ozone depletion of 5 % has been observed by TOMS about two years after the eruption after removing the effect of the quasi-biennial oscillation (QBO) (Randel et al., 1995). Changes of similar magnitude have been obtained in modelling studies (Kinnison et al., 1994; Bekki and Pyle, 1994), and were attributed to enhanced heterogeneous ozone-depleting reactions on sulphate aerosols and changes in circulation due to stratospheric aerosol heating. Stratospheric ozone loss would lead to an increase of UV radiation in the troposphere, and thus to a higher OH abundance and a shorter methane lifetime.

The eventual fate of the volcanic sulfur is deposition to the surface. The modelling results of Gauci et al. (2008) indicate that deposition of 122 Tg SO_2 emitted by the Laki eruption lead to a decrease of 8.8 Tg yr^{-1} in methane emissions from wetlands in the

two years following the eruption. As a rough estimate assuming linearity, the Pinatubo eruption would lead to 1.3 Tg decrease in the emissions. We consider this effect to be small and do not investigate it further here.

Other effects of the eruption on methane have occurred because of temperature changes after the eruption (Bekki and Law, 1997). The scattering of shortwave radiation by aerosols led to an increase in the reflected solar radiation of up to 10 $W m^{-2}$ at the top of the atmosphere (Bender et al., 2010). This affected tropospheric temperatures, leading to an observed global cooling by up to 0.45 °C in the two years following the eruption (Free and Angell, 2002). Bender et al. (2010) show that ten general circulation models give a maximum decrease of 0.5 °C in response to the observed changes in the shortwave radiative flux after the eruption. They attribute the 0.05 °C difference between models and observations to the coinciding El Niño event.

Temperature changes trigger changes in the chemical composition of the atmosphere, as well as in natural sources related to biogenic activity. A decrease in temperature would generally slow down photochemical transformations. In particular, the slowdown of the reaction between methane and OH would lead to higher tropospheric methane concentrations (Bekki and Law, 1997). In the study of Soden et al. (2002) it is found that the cooling after the eruption is associated to a maximum global decrease of 3 % in the water vapour column in both observations and model simulations. Less water vapour in the troposphere would imply less OH formation from ozone, because of the intermediate reaction of $O(^1D)$ with water. This would increase the methane lifetime, leading to methane build-up in the atmosphere. Natural emissions from wetlands, accounting for about 30 % of the total emissions in the year 2004 (Spahni et al., 2011), are sensitive to temperature and soil moisture changes. Furthermore, natural emissions of NMVOC are known to be temperature dependent (Guenther et al., 1993). A decrease of the surface temperature would result in a reduction of both methane emissions from wetlands and biogenic NMVOC emissions. Biogenic emissions of NMVOC are also dependent on the amount of photosynthetically active radiation (PAR) reaching the surface (Guenther et al., 1993). Decrease in PAR fluxes because of enhanced aerosol

scattering would further decrease these emissions. While a reduction in methane emissions directly impacts methane concentrations, a decrease in NMVOC emissions may have an effect on OH, and thus impose an indirect impact on the methane lifetime.

The eruption of Pinatubo also had impacts on the dynamics of the atmosphere, which might have influenced OH and methane concentrations. It was inferred in the 4-box modelling study of Schauffler and Daniel (1994) that heating of the stratosphere may increase the exchange between the stratosphere and the troposphere, leading to a decrease in tropospheric methane concentrations. However, Lowe et al. (1997) suggest that a large effect of enhanced stratosphere-troposphere exchange would be inconsistent with the decrease in $\delta^{13}C$ observations in this period.

Although the processes presented above are known to have contributed to the evolution of the methane growth rate after the Pinatubo eruption, their relative magnitudes are still unclear. Methane observations show the net outcome of these processes and other processes not related to the eruption, such as changes in anthropogenic emissions. The growth rate changes after the eruption have been attributed in other studies to changes in either sources or sinks. Dlugokencky et al. (1994) relate the decrease in methane growth rate in 1992 to a decrease in anthropogenic emissions. Dlugokencky et al. (1996) show that the methane and CO evolution in 1991 and early 1992 is consistent with a decrease in OH for up to a year after the eruption. The modelling study of Bekki and Law (1997) shows that the growth rate of methane in 1991/1992 can be explained by reduced emissions from wetlands. The inverse modelling study of Butler et al. (2004) reveals a global source-sink imbalance of 27 Tg methane for the year 1991 and –19 Tg for the year 1992. In their inverse modelling studies, Bousquet et al. (2006) and Wang et al. (2004) both find a decrease in wetland emissions of 20–25 Tg. between 1991 and 1993. Bousquet et al. (2006) also find reductions in the biomass burning and anthropogenic emissions, as well as in the OH sink for this period. In contrast, Wang et al. (2004) postulate an increase in OH due to reduced stratospheric ozone. Using a two-dimensional model, Bekki et al. (1994) conclude that half of the methane growth rate reduction in 1992 can be attributed to the effect of decreased stratospheric ozone.

In the modelling study of Telford et al. (2010) it is found that natural isoprene emissions have a minimum in early 1993, yielding an increase in the methane sink of 5 Tg yr^{-1}. Telford et al. (2010) also show that variations in meteorology lead to a decrease in the methane sink of up to 14 Tg yr^{-1}, mainly due to changes in temperature and water vapour following the eruption. To our knowledge, no complete study has been made to include all competing effects of the Pinatubo eruption and to analyze the processes responsible for OH and methane growth rate variations. Quantifying these processes may help us gain a better understanding of the methane budget and, consequently, to make better predictions of the future atmospheric burdens.

In this study we will use a simplified tropospheric column chemistry model to assess the changes in the methane growth rate after the Pinatubo eruption and the relative contributions of the various processes. First, we will analyse how the steady state of the chemical system changes when varying individual conditions (emissions, photolysis frequencies, water vapor). The impact on the equilibrium state of the tropospheric column gives us an idea about the drivers of methane and OH concentrations, and about the relative magnitude of different processes. Next, this evolution is contrasted to a transient simulation, in which the system is not allowed to reach a steady state, but responds to transient perturbations. This will show that not only the magnitude of the perturbation plays a role, but also the duration. Due to limitations of the model, the effect of changes in the dynamics of the atmosphere are not studied here. Since isoprene constitutes more than 80 % of the biogenic NMVOC emissions, only changes in isoprene emissions will be included in the steady-state perturbations.

A detailed description of the column chemistry model is presented in Sect. 2. In Sect. 3.1 we show sensitivities of the model, and evaluate its performance in representing the global atmosphere in the period 1890–2005. We show our results on steady-state and transient methane changes after Pinatubo in Sect. 3.2, and conclusions are drawn in Sect. 4.

2 Model setup

The model used in this study is a one-dimensional column chemistry model, coupled to the radiation model TUV (Madronich, 1993, http://cprm.acd.ucar.edu/Models/TUV/). The chemistry model can be used both in steady-state and transient versions. The effects of atmospheric perturbations on photolysis frequencies are calculated with the radiative transfer model TUV, and then employed in the chemistry model.

2.1 The column chemistry model

In this exploratory study we use a strongly simplified model that represents the troposphere in 10 vertical layers of 1.5 km thickness each. The chemical scheme employs 8 chemical species, of which 5 are transported between adjacent layers (O_3, NO_x, CH_4, CO, RH). OH, HO_2 and RO_2 are not transported, but calculated in steady state with the longer-lived transported species. Here RH stands for NMVOC, and RO_2 for peroxy-radicals formed from NMVOC and methane oxidation.

Vertical transport is defined by vertical diffusivity factors of 5 m^2 s^{-1} between the first two layers (at 1.5 km), 2 m^2 s^{-1} between the second and 3rd layers (at 3 km) and 1 m^2 s^{-1} higher up. No flux to the stratosphere is considered except for ozone and methane. For ozone, we fix the concentration in the upper layer (at 13.5 km) at 81 ppb. A flux of 40 Tg yr^{-1} to the stratosphere is considered for methane, following Prather et al. (2001).

The chemical reactions included are presented in Table 1. We run our model with all-day all-year averaged reaction rates and photolysis frequencies. The 0.9 CO yield from methane oxidation is comparable to that found by complex 3-D global chemistry models (Shindell et al., 2006). The yield of CO from the oxidation of NMVOC varies greatly between species (Grant et al., 2010). We use here a global CO yield from NMVOC of 0.5. Methane oxidation produces CH_3O_2, which may react with NO, producing at least one molecule of HO_2 through all the reaction pathways. CH_3O_2 is included in the model as RO_2, together with other compounds produced from NMVOC oxidation. Thus an

HO_2 yield y from the reaction of RO_2 and NO is considered, equal to the ratio between the CH_3O_2 production from methane and the total RO_2 production. For computational reasons, we use a global yield determined using a steady-state assumption. The rate of production of CH_3O_2 from methane oxidation is equal to the rate of loss of methane in this reaction. Assuming steady state, this is equal to the emission rate of methane (E_{CH4}). Similarly, the rate of RO_2 production from NMVOC is equal to the emission rate of NMVOC (E_{RH}). Therefore y is taken as $\frac{E_{CH4}}{E_{CH4}+E_{RH}}$.

Dry deposition of ozone and NO_2 are included with a deposition velocity of $1.0 \times 10^{-3}\,m\,s^{-1}$, and an additional loss of NO_2 through heterogeneous reactions is considered, with a velocity of $1.5 \times 10^{-4}\,m\,s^{-1}$ throughout the column.

We track the steady state under changing conditions by implementing the model in the AUTO software for continuation and bifurcation (Doedel et al., 2001). This software tracks the steady state of a system of ordinary differential equations as a function of a certain parameter, such as emissions or photolysis frequencies. Our system of 8 chemical species and 10 vertical layers leads to 80 coupled equations with 80 unknowns to be solved by AUTO.

A time-dependent version of the chemistry model performs transient simulations using the Euler Backward Iterative scheme with a time step of one hour.

2.2 Photolysis frequencies

The TUV model version 4.1 is used to calculate the effects of SO_2, aerosols and ozone column on tropospheric photolysis frequencies. Yearly averaged photolysis frequencies are calculated by averaging daily averaged photolysis frequencies at 20° N for the 15th of the months of March, June, September and December. This latitude band is used because photochemistry is most active in the tropics, and in order to have a good representation of the four seasons.

For the base scenario, the climatological aerosol profile of Elterman (1968) is used, with an aerosol single scattering albedo of 0.99.

2.3 Emissions and atmospheric parameters

Global anthropogenic emissions for NO_x, CO, methane and NMVOCs are taken from EDGAR 4.1 yearly values for the years 1970–2005 (European Commission and Joint Research Centre (JRC)/Netherlands Environmental Assessment Agency (PBL), 2010), and EDGAR-HYDE decadal emissions for the years 1890–1970 (Van Aardenne et al., 2001). Natural emissions used are described in Huijnen et al. (2010), except for methane emissions, which are taken from Spahni et al. (2011) posterior values. To obtain a smooth variation in emissions, we interpolate the NO_x and CO emission data by a 6th degree polynomial, and the methane and NMVOC emissions by a 7th degree polynomial. The evolution of methane emissions implemented in the model is shown in Fig. 3.

In addition to surface NO_x emissions, we add yearly 5 Tg N of NO_x from lightning, evenly distributed throughout the column.

Profiles of temperature, water vapour, ozone, and air density for 20° N were derived from the global 3-D chemistry transport model TM5 (Huijnen et al., 2010) driven by ERA Interim meteorological fields (Dee et al., 2011) for the year 2005. These are applied both in TUV and in the column chemistry model. The ozone columns for the four months used here are respectively 325, 328, 330 and 295 Dobson Units (DU).

2.4 Implementation of Pinatubo perturbations

The perturbations implemented in TUV and the column chemistry model are summarised in Table 2. To compute the perturbations in photolysis frequencies and PAR flux after Pinatubo in TUV, we implement single forcings of 5 % decrease in ozone column, 2.54 DU increase in SO_2, equivalent to 18.5 Tg SO_2, and 0.15 increase in AOD. SO_2 and aerosols are considered to be evenly distributed around the world and between 15 and 30 km altitude. In the column chemistry model, the perturbations in photolysis frequencies and PAR flux are then scaled with the magnitudes of the forcing, thus assuming that the effects of these processes are linear. In addition, we assume

additivity between the different processes by adding the perturbations in photolysis frequencies and PAR flux when more than one process is considered. We tested the effect of this assumption on our results, by performing two simulations: one in which we used photolysis rates calculated with TUV by implementing all the forcings at the same time, and one in which we implemented each forcing separately and assumed additivity. The difference in the surface methane steady-state concentration between the two simulations is 0.5 ppb, which is small compared to the magnitude of the perturbations related to the eruption.

The time evolution of the forcings assumed in the column chemistry model is based on observed values, and is shown in Fig. 1. For SO_2, we consider an exponential decay with an e-folding time of 24 days and a starting global mean concentration of 2.54 DU directly after the eruption. For the aerosol optical thickness and surface temperature changes, we interpolate the GISS monthly averaged data (Hansen et al., 2010; Thomason et al., 1997) in the 4.5 and 3.5 yr following the eruption, respectively. The resulting evolution has a peak at approximately 7 and 15 months after the eruption, respectively, and then a smooth decay, which is extended for 10 yr. To a 0.5 °C temperature decrease at the surface, we associate a tropospheric temperature change of 0.5 °C decrease below 214.4 mbar, and a 1 °C increase at 87.7 mbar, following the observations from Free and Angell (2002), and interpolate between these values. These profile changes are then scaled with the magnitude of the surface temperature change. For ozone decrease, we also use an evolution that has a peak of 4.5 % two years after the eruption and then decays to 0, following the results of Randel et al. (1995).

The water vapour profile as a function of temperature change is evaluated using the Clausius Clapeyron equation, assuming constant relative humidity. Variations in emissions of methane from wetlands due to temperature are calculated using the Q10 temperature dependence relation (Dunfield et al., 1993), with a Q10 value of 2. For a temperature decrease of 0.5 °C, we find that methane wetland emissions decrease from 171.8 Tg yr^{-1} to 165.9 Tg yr^{-1}. The isoprene emission changes are computed by

using the MEGAN-like dependence on temperature and PAR flux emission as in Guenther et al. (1993).

All the perturbations are implemented both in the steady-state and transient versions of the model, starting with 1990 steady-state concentrations. We compare the effect of the eruption to the effect of variations in anthropogenic sources by performing two additional transient simulations. In the first one we employ variable yearly anthropogenic emissions from EDGAR 4.1, while keeping the biomass burning emissions constant to 1990 values. In the second one we include variable anthropogenic emissions, fixed biomass burning emissions, as well as the forcing of the eruption. These later two simulations are performed starting from the steady state in the year 1890, using EDGAR-HYDE emissions for the spin-up period between 1890 and 1970.

3 Results and discussion

3.1 Model sensitivities

Even though the model presented above contains many simplifications, we will show below that the model performs reasonably well in representing the global state of the troposphere. In this respect, we present a series of sensitivities and make comparisons with values found in the literature.

Figure 2 shows the steady-state profiles for methane, O_3, NO_x, and CO obtained by the steady-state model for the years 1890 and 1990. The yearly emission values used are shown in Table 3. Surface concentrations found by our model fall well within the range of observations. Methane in the year 1990 decreases with altitude by about 200 ppb throughout the troposphere. CO concentrations for the same year decrease with altitude from 160 ppb at the surface to 20 ppb near the tropopause. The NO_x profile has the typical C-shape due to the emissions by lightning and the longer lifetime of NO_x in the upper troposphere. Ozone in the boundary layer is produced from NO_x and hydrocarbons, while higher up it is mostly determined by the stratospheric boundary

condition. This leads to a decrease with respect to altitude in the first few kilometers, and then an increase towards the stratosphere.

Between the years 1890 and 1990, we find increases in ozone, CO and methane, which are more pronounced near the surface due to increases in emissions. For NO_x we find increases both near the surface, because of increased emissions, as well as near the tropopause, due to an increase in the NO_x lifetime at this altitude. This is consistent with a decrease in OH at this altitude due to higher methane. In the study of Wang and Jacob (1998), zonal averaged profiles for ozone, OH, NO_x and CO are computed using a three-dimensional model of tropospheric chemistry for the preindustrial and year 1990 conditions. Concentrations of ozone and NO_x near the surface are somewhat higher in our model, possibly due to the fact that no differentiation is made between land and ocean in our simplified single column model. Their values for CO show also much less variability throughout the column, possibly due to the fact that we did not formulate a convective redistribution of the column. In terms of changes in concentrations between preindustrial setup and the year 1990, our model finds generally lower relative changes than the study of Wang and Jacob for O_3, NO_x and CO, possibly be due to the different emission sets that are used. However, the 38 % increase in OH that we find in the first layer, and about 20 % decrease between 6 and 12 km altitude compare well with their study.

In Table 4, we compare the ozone, OH and CO budgets given by our model for the year 1990 to global budgets found by several 3-dimensional chemistry transport models presented in the papers of Williams et al. (2012); Stevenson et al. (2006); Shindell et al. (2006). Overall, our model falls within the uncertainties of these models in terms of OH and CO burdens and budgets. CO and methane lifetimes are also modeled realistically, certainly when one considers the huge simplifications of the chemical system and the simplified representation of the global atmosphere. Ozone production and deposition are quite high, likely due to the choice of tropical conditions to represent the global troposphere.

We further verify the sensitivity of the model to changes in the methane emissions. The effect of methane emission changes on the methane concentration is enhanced by the feedback via the methane lifetime. To describe this process, a feedback factor a can be defined as $\frac{d\mathrm{CH_4}}{\mathrm{CH_4}} = a\frac{dE_{\mathrm{CH4}}}{E_{\mathrm{CH4}}}$, where $d\mathrm{CH_4}$ stands for the small perturbation in the methane concentration determined by a small perturbation dE_{CH4} in methane emissions. We find that a has a value of 1.37 for the year 1990, which falls within the range of 1.2–1.6 found in the Second Assessment Report of the IPCC (Prather et al., 1996). Isaksen et al. (2011) also finds a feedback factor of 1.5 for an increase of 100 Tg in methane emissions. Furthermore, the recycling probability of OH, defined by differentiating between the OH primary production from ozone photolysis and secondary production from recycling processes (Lelieveld et al., 2002), is 0.41. This is slightly lower than the global mean value of 0.5 found by Lelieveld et al. (2002), likely due to the relatively high water vapour concentrations in the tropospheric profiles used here.

Another sensitivity that is important to our study is the sensitivity of methane to changes in the ozone column. Our model gives a sensitivity factor of tropospheric methane to changes in ozone column of –1.57. This means that a 1 % increase in the ozone column leads to a 1.57 % decrease in tropospheric methane. This sensitivity is found to be –0.98 in the study of Camp et al. (2001), using observations of methane from Cape Grimm station, and ozone columns from TOMS between 40–45° S. Using a two-dimensional model Fuglestvedt et al. (1994) estimate this factor to be –0.79. Similarly, our model calculates a sensitivity factor of tropospheric OH to changes in ozone column of 1.69, compared to other studies that find values between 0.7 and 0.99 (Camp et al., 2001). The differences are most likely caused by the relatively high temperature and water vapour used in our model. We selected an atmospheric column close to the tropics, because the photochemical activity, important for the methane budget, is high in the tropics. Our compromise leads to a relatively large sensitivity of methane to stratospheric ozone compared to full 3-D models. Given these sensitivities, results should be interpreted with care.

Evolution of methane in the last century

We test the performance of the model in simulating methane concentrations in the period 1890–2005. Both steady-state and transient results for surface methane are compared in Fig. 3 to global means for the period 1890 to 1990 calculated from ice core measurements in Etheridge et al. (1998). Following the same procedure as used in this study, we estimate global mean concentrations for the period 1985 to 2005 based on the monthly mean data from the NOAA stations at Alert and South Pole. The global mean is therefore computed as the concentration at South Pole plus 37 % of the interpolar difference. The evolution of the steady state generally follows the evolution of methane emissions up to the year 1980. After 1980 we find a decrease in the steady state, and a subsequent recovery after the year 2000. This is probably due to a stabilization in the sources of methane while NO_x emissions continue to increase. The transient results follow the steady states with a delay of about 8 yr, due to the methane lifetime. The temporary decrease in the steady state coincides with a stabilization of the transient concentrations, a phenomenon that has been observed in the atmospheric methane concentrations (Dlugokencky et al., 2003). Compared to the observations, our model generally overestimates methane concentrations. We expect this to happen in the first decades of the simulation, because the starting point represents a steady state, while the system might not have been in a steady state in the year 1890. The concentration continues to be overestimated until 1990, pointing either to an overestimation of the methane emissions or an underestimation of the methane lifetime in this period. However, the modelled transient concentration becomes close to the observed values in 1990–2005, which is the period we are interested in.

3.2 The Pinatubo Eruption

3.2.1 Steady-state perturbations

We test the effect of each of the forcings of the Pinatubo eruption described in Table 2 on the methane steady-state, using the maximum magnitude of each forcing. The differences in surface methane and tropospheric OH between each simulation and the "base" simulation are shown in Fig. 4.

We find that the 5 % reduction in ozone column has the largest effect on the surface methane equilibrium concentration, decreasing it by 125 ppb. SO_2, aerosol, water vapour and isoprene changes all increase the methane steady-state by 40 to 60 ppb. The effects of temperature decrease on methane emissions and reaction rates have smaller impacts on the simulated steady-state concentrations, of 27 and 15 ppb repectively. The temperature-related processes, that is "Temp Rates", "H_2O", "Methane Emis" and "Isoprene Emis", mostly cancel each other out, resulting in an overall decrease of 10 ppb.

Except for the effects of changed methane emissions and changed reaction rates, the effects on methane are strongly correlated to effects on OH of the same relative magnitude and of opposite sign. The OH response to decreasing methane emissions reflects the effectiveness of the feedback factor introduced in the previous section. Changed reaction rates due to tropospheric cooling lead to a small increase in OH, because of slower oxidation rates of methane, CO, and NMVOC.

We find a maximum decrease in isoprene emissions of 9 %. This compares well with the findings by Telford et al. (2010). However, the change in OH found by our column chemistry model is 3 %, much larger than the 1 % change in OH found by the aforementioned study. A more recent study shows that the effect of aerosols on isoprene emissions is smaller if diffuse and direct radiation is treated separately (Wilton et al., 2011). The overestimation of our model might be due to the fact that we are not able to represent horizontal transport mechanisms. Isoprene reacts rapidly with OH and regions with large and small isoprene emissions are present in the true atmosphere.

Furthermore, the CO yield from NMVOC of 0.5 used in our model might be high compared to the isoprene yield, leading to high OH sensitivity. We conclude therefore that the calculated feedback of NMVOC emissions on OH is overestimated by our column model, and we do not include it in further simulations. We simply note that decreases in NMVOC emissions probably lead to more OH and a smaller methane lifetime.

Concerning the effect of temperature and water vapour, Telford et al. (2010) also find that they reduce OH by maximum 2.5 %, in good agreement with the 3 % found here.

3.2.2 Evolution of steady-state and transient concentrations

The forcings presented above not only have different effects on the methane steady-state concentrations, but acted at different moments in time after the eruption and at different timescales. The evolution of the steady-state methane concentrations (Fig. 5a) reflects the change in the balance between methane sources and sinks. The overall effect obtained is a positive jump in the steady-state concentrations immediately after the eruption, because of the injection of SO_2. The effect on the steady state remains remains positive, reflecting a decrease in the methane sink because of sulphate aerosols for up to 6 months after the eruption. After that, the ozone effect starts to dominate. Partly counteracted by other effects, it determines a maximum steady-state decrease of 70 ppb two years after the eruption.

While the steady state reacts instantaneously to perturbations in sources or sinks, the effect on transient concentrations also depend on the methane lifetime. Because the methane lifetime is about 8 yr, the concentration at one moment in time shows an integrated effect of perturbations to its steady state in the previous years. Therefore not only the magnitude, but also the duration of the perturbation plays an important role in determining the result.

The modelled transient concentration of surface methane (Fig. 5b) slightly increases for 1–2 months after the eruption, then decreases, reaching a maximum decrease of 15 ppb about 5 yr after the eruption. The maximum effect on methane concentrations occurs later, and is smaller than the effect on the steady state. Also the recovery time to

initial concentrations is much longer compared to the recovery time of the perturbations applied. The SO_2 effect is hardly observed in the transient concentrations, because of its short duration. All the other processes are seen to affect the methane concentration for up to 40 yr after the eruption. The difference between the results for the steady-state and transient methane concentrations, in both Figs. 5 and 3, show that a steady-state assumption for methane does not hold on yearly and decadal timescales.

3.2.3 Growth rate evolution

The overall effect of the Pinatubo forcings on the surface methane growth rate (Fig. 6a) is a positive jump of 6 ppb yr^{-1} due to UV absorption by SO_2 immediately after the eruption. The effect decreases, but remains positive for about half a year after the eruption due to the presence of SO_2 and sulphate aerosols in the stratosphere. After that, the effect on the methane growth rate is dominated by the forcing exerted by ozone depletion, partly counteracted by decreased water vapour. We find that the effect of the eruption on methane growth rate experiences a minimum of –6 ppb yr^{-1} about 2 yr after the eruption. The growth rate increases afterwards, reaching zero about 5 yr after the eruption, at the moment when the effect on the transient methane concentrations is at a minimum (Fig. 5b). The slow recovery of the concentrations to the steady state is marked by a small positive growth rate of less than 1 ppb yr^{-1}. The shape of the growth rate evolution is somewhat similar to the shape of the steady-state evolution, because they both reflect the annual balance between methane sources and sinks.

We find a possitive methane growth rate due to decreased OH for about one year after the eruption, in agreement with Dlugokencky et al. (1996). The large effect of ozone depletion which follows compares well with the results of Bekki et al. (1994). They report a 7 ppb yr^{-1} decrease in growth rate from spring 1991 to autumn 1992 due to ozone depletion. Similar to our results, Bousquet et al. (2006) find an increase in the OH sink until the beginning of 1992, and then a subsequent decrease in 1992 and 1993. However, they find different magnitudes of these changes than us, leading to an overall increase in the OH sink between 1991 and 1993. The magnitude of the

temperature-related effects that we find compares well with the ones shown in Bekki and Law (1997). We find a maximum of 6 Tg yr^{-1} change in wetland emissions after the eruption. This is similar to the bottom up estimate of about 5 Tg yr^{-1} in Spahni et al. (2011), but a few times lower than the maximum anomaly of about 40 Tg yr^{-1} found in the inverse modelling study of Bousquet et al. (2006). Our lower estimate might be partly due to the fact that we considered here changes in methane emissions solely due to temperature. Methane emission changes also depend on spatial and temporal changes in soil moisture and precipitation, which have also been observed after the eruption (Spahni et al., 2011). Changes in wetland extent were also shown to have a large impact on the interannual variability in methane emissions from wetlands (Ringeval et al., 2010), which is also not taken into account in the study of Spahni et al. (2011) for the years following the eruption. In addition, we consider a global Q10 factor of 2, while this factor was shown to be dependent on ecosystem type, with a range of measured values between 1.6 and 16 (Dunfield et al., 1993; Valentine et al., 1994).

The modelled growth rate with varying anthropogenic emissions of methane, CO, NO_x and NMVOC, and the comparison of our results with NOAA observations are shown in Fig. 6b. Methane anthropogenic emissions are relatively stable in the years 1990 and 2000, while anthropogenic NO_x emissions increase and CO emissions decrease. Therefore when only variations in anthropogenic emissions are taken into account, we find a generally decreasing trend in methane growth rate due to a decrease in methane lifetime. The growth rate found with our column chemistry model is generally lower than the observed one, possibly due to an underestimation of the methane lifetime in this period or an overestimation of the methane emissions. The fact that changes in anthropogenic emissions partly contributed to the observed decrease in methane growth rate between 1991 and 1993 and the increase in 1997–1998 is in agreement with previous studies (Dlugokencky et al., 1994; Bousquet et al., 2006).

When both anthropogenic emissions and the Pinatubo forcings are included, we find a general correspondence between the modelled growth rate and the observed one in the years 1991 to 1996. However, the increased growth rate in 1994 is not

captured in our results. Decreased methane emissions between the years 1991 and 1993 are found to contribute by an additional 5 ppb yr^{-1} to the drop in methane growth rate in this period. The timing of the minimum growth rate after the eruption is modelled about 9 months later than that observed. The difference between the modelled and the observed growth rate are most likely due to other processes not included here, that are known to determine methane variability. Such processes include changes in biomass burning emissions (Bousquet et al., 2006) and variability in wetland emissions due to atmospheric changes related to the El Niño Southern Oscillation (ENSO) cycle (Hodson et al., 2011). Differences between the modelled and observed growth rate curves may arise also from the interpolation procedure used to obtain the observed global methane growth rate curve.

By comparing the sum of the "Pinatubo all" and "Anthrop" curves to the growth rate evolution when including both Pinatubo forcings and changes in anthropogenic emissions, we can find the role of second order effects. Generally, we find that the effect of nonlinearity on growth rates is less then 10 %.

In order to show that our results are robust with respect to the model setup, we performed a series of sensitivity tests. We tested different temperature and water vapour profiles, a lower value for the CO yield from the oxidation of NMVOC, including NMVOC recycling, and increased vertical mixing. Although the effect on the modelled methane concentrations in the last century may be in the order of 100 ppb (results not shown), the effect on the growth rate evolution after the eruption is less than 10 %. Changing the temperature by –2.5 °C to +1 °C and simultaneously changing the water vapour profile according to the Clausius-Clapeyron equation lead to changes in the methane growth rate results of less than 0.1 ppb yr^{-1}. Similar results are obtained when changing the CO yield from NMVOC to 0.3 instead of 0.5. Including a 0.25 yield of HO_2 from the oxidation of NMVOC in the presence of NO_x, and doubling the vertical mixing coefficients lead to a higher growth rate minimum after the eruption by respectively 0.3 and 0.6 ppb yr^{-1}. We estimate therefore a maximum error of 15 % in the modelled growth rate due to the model setup.

Horizontal distributions of the modelled forcings can play an important role in the effect on the methane growth rate, and cannot be simulated in our column model. We expect that the effect of SO_2 is overestimated in our results, by inferring an instant homogenisation of the emissions. In reality, high concentrations were found close to the emission point after the eruption, and afterwards the short lifetime caused the dispersion of SO_2 only at low latitudes with a nonuniform horizontal distribution (Guo et al., 2004). Changes in stratospheric aerosol, ozone and temperature have been observed globally, but with different magnitudes at different latitudes. Since photolysis is more important in the tropics, processes that are larger in the tropics will have a higher impact.

Nonetheless, we quantified for the first time the combined effect of radiation and temperature-related effects of the Pinatubo eruption on the methane growth rate including feedbacks on the methane lifetime.

4 Conclusions

We have implemented a column chemistry model, and tested its performance in representing the mean state of the atmosphere. Using this model, we are able to investigate the sensitivities of methane steady-state and transient concentrations to atmospheric and emission perturbations following the volcanic eruption of Pinatubo. We find that full recovery of transient methane concentrations takes about 40 yr.

The modelled evolution of the methane growth rate shows a remarkable comparison with the observations, considering the simplicity of our model. We conclude that a multitude of emission and lifetime effects contributed to the observed growth rate variations following the eruption. The dominating effects are those through tropospheric photolysis rates, with ozone depletion having the largest effect. This shows the importance of stratospheric-tropospheric couplings, and that a good representation of stratospheric chemistry is needed in order to model accurately methane concentrations. We also find

that the decrease in anthropogenic emissions between 1991 and 1993 contributed to the decreased methane growth rate in 1993.

Our model has the advantage of simplicity, however there are processes that cannot be represented, such as horizontal transport and changes in the dynamics of the atmosphere. Also, we did not consider spatial distributions of methane emissions. Using a global vegetation model would give better estimates of the the response of natural emissions to changes in temperature, precipitation and radiation. Therefore, a three dimensional chemistry transport model coupled with a climate model will be used to perform future experiments.

Acknowledgements. This work was supported by the Netherlands Organisation for Scientific Research (NWO) and the EU FP7 Integrated Project PEGASOS. We thank the NOAA global air sampling network for their efforts in gathering the methane measurements and the GLOBALVIEW methane project for extending and integrating the data.

References

Bekki, S. and Law, K. S.: Sensitivity of the atmospheric CH_4 growth rate to global temperature changes observed from 1980 to 1992, Tellus, 49, 409–416, 1997. 18031, 18033, 18034, 18047

Bekki, S. and Pyle, J. A.: A two-dimensional modeling study of the volcanic eruption of Mount Pinatubo, J. Geophys. Res., 99, 18861–18869, 1994. 18032

Bekki, S., Law, K. S., and Pyle, J. A.: Effect of ozone depletion on atmospheric CH_4 and CO concentrations, Nature, 371, 595–597, 1994. 18034, 18046

Bender, F. A., Ekman, A. M. L., and Rodhe, H.: Response to the eruption of Mount Pinatubo in relation to climate sensitivity in the CMIP3 models, Climate Dynamics, 35, 875–886, doi:10.1007/s00382-010-0777-3, 2010. 18033

Bousquet, P., Ciais, P., Miller, J. B., Dlugokencky, E. J., Hauglustaine, D. A., Prigent, C., Van der Werf, G. R., Peylin, P., Brunke, E.-G., Carouge, C., Langenfelds, R. L., Lathière, J., Papa, F., Ramonet, M., Schmidt, M., Steele, L. P., Tyler, S. C., and White, J.: Contribution of anthropogenic and natural sources to atmospheric methane variability., Nature, 443, 439–443, doi:10.1038/nature05132, 2006. 18031, 18034, 18046, 18047, 18048

Butler, T. M., Simmonds, I., and Rayner, P. J.: Mass balance inverse modelling of methane in the 1990s using a Chemistry Transport Model, Atmos. Chem. Phys., 4, 2561–2580, 2004, http://www.atmos-chem-phys.net/4/2561/2004/. 18031, 18034

Camp, C. D., Roulston, M. S., Haldemann, A. F., and Yung, Y. L.: The sensitivity of tropospheric methane to the interannual variability in stratospheric ozone, Chemosphere - Global Change Science, 3, 147–156, doi:10.1016/S1465-9972(00)00053-2, 2001. 18042

Dee, D. P., Uppala, S. M., Simmons, A. J., Berrisford, P., Poli, P., Kobayashi, S., Andrae, U., Balmaseda, M. A., Balsamo, G., Bauer, P., Bechtold, P., Beljaars, A. C. M., Berg, L. V. D., Bidlot, J., Bormann, N., Delsol, C., Dragani, R., Fuentes, M., Geer, A. J., Haimberger, L., Healy, S. B., Hersbach, H., Holm, E. V., Isaksen, L., and Kallberg, P.: The ERA-Interim reanalysis: configuration and performance of the data assimilation system, Q. J. Roy. Meteor. Soc., 137, 553–597, doi:10.1002/qj.828, 2011. 18038

Dlugokencky, E. J., Masaire, K. A., Lang, P. M., Tans, P. P., Steele, L. P., and Nisbet, E. G.: A dramatic decrease in the growth rate of atmospheric methane in the Northern Hemisphere during 1992, Geophys. Res. Lett., 21, 45–48, 1994. 18031, 18034, 18047

Dlugokencky, E. J., Dutton, E. G., Novelli, P. C., Tans, P. P., Masarie, K. A., Lantz, K. O., and Madronich, S.: Changes in CH_4 and CO growth rates after the eruption of Mt. Pinatubo and their link with changes in tropical propospheric UV flux, Geophys. Res. Lett., 23, 2761–2764, 1996. 18031, 18032, 18034, 18046

Dlugokencky, E. J., Houweling, S., Bruhwiler, L., Masarie, K. A., Lang, P. M., Miller, J. B., and Tans, P. P.: Atmospheric methane levels off: temporary pause or a new steady-state?, Geophys. Res. Lett., 30, 1992, doi:10.1029/2003GL018126, 2003. 18031, 18043

Dlugokencky, E. J., Nisbet, E. G., Fisher, R., and Lowry, D.: Global atmospheric methane: budget, changes and dangers, Phil. Trans. R. Soc. A, 369, 2058–2072, doi:10.1098/rsta.2010.0341, 2011. 18030

Doedel, E. J., Paffenroth, R. C., Champneys, A. R., Fairgrieve, T. F., Kuznetsov, Y. A., Sandstede, B., and Wang, X.: AUTO 2000: continuation and bifurcation software for ordinary differential equations (with HomCont), Tech. rep., Caltech, 2001. 18037

Dunfield, P., Knowles, R., Dumont, R., and Moore, T. R.: Methane production and consumption in temperate and subarctic peat soils: response to temperature and pH, Soil Biol. Biochem., 25, 321–326, http://www.sciencedirect.com/science/article/pii/0038071793901304, 1993. 18039, 18047

Elterman, L.: UV, visible and IR attenuation for altitudes to 50 km, Environ. Res. Papers, 285, AFCRL-68-0153, 1968. 18037

Etheridge, D. M., Steele, L. P., Francey, R. J., and Langenfelds, R. L.: Atmospheric methane between 1000 A. D. and present: evidence of anthropogenic emissions and climatic variability, J. Geophys. Res., 103, 15979–15993, 1998. 18043, 18063

European Commission and Joint Research Centre (JRC)/Netherlands Environmental Assessment Agency (PBL): Emission Database for Global Atmospheric Research (EDGAR), release version 4.1, http://edgar.jrc.ec.europa.eu/, 2010. 18038

Free, M. and Angell, J. K.: Effect of volcanoes on the vertical temperature profile in radiosonde data, J. Geophys. Res., 107, 4101, doi:10.1029/2001JD001128, 2002. 18033, 18039

Fuglestvedt, J. S., Johnson, J. E., and Isaksen, I. S. A.: Effects of reductions in stratospheric ozone on tropospheric chemistry through changes in photolysis rates, Tellus, 46, 172–192, 1994. 18042

Gauci, V., Blake, S., Stevenson, D. S., and Highwood, E. J.: Halving of the northern wetland CH_4 source by a large Icelandic volcanic eruption, J. Geophys. Res., 113, 1–8, doi:10.1029/2007JG000499, 2008. 18032

GLOBALVIEW-CH4: Cooperative Atmospheric Data Integration Project - Methane. CDROM, NOAA ESRL, Boulder, Colorado, available at: ftp://ftp.cmdl.noaa.gov, Path: ccg/ch4/GLOBALVIEW, 2009. 18066

Grant, A., Archibald, A. T., Cooke, M. C., and Shallcross, D. E.: Modelling the oxidation of seventeen volatile organic compounds to track yields of CO and CO_2, Atmos. Environ., 44, 3797–3804, doi:10.1016/j.atmosenv.2010.06.049, 2010. 18036

Guenther, A. B., Zimmerman, P. R., Harley, P. C., Monson, R. K., and Fall, R.: Isoprene and monoterpene emission rate variability: model evaluations and sensitivity analyses, J. Geophys. Res., 98, 12609–12617, 1993. 18033, 18040

Guo, S., Bluth, G. J. S., Rose, W. I., Watson, I. M., and Prata, A. J.: Re-evaluation of SO_2 release of the 15 June 1991 Pinatubo eruption using ultraviolet and infrared satellite sensors, Geochem. Geophys. Geosys., 5, Q04001, doi:10.1029/2003GC000654, 2004. 18032, 18049

Hansen, J., Ruedy, R., Sato, M., and Lo, K.: Global surface temperature change, Rev. Geophys., 48, RG4004, doi:10.1029/2010RG000345, 2010. 18039

Hodson, E. L., Poulter, B., Zimmermann, N. E., Prigent, C., and Kaplan, J. O.: The El Niño Southern Oscillation and wetland methane interannual variability, Geophys. Res. Lett., 38, 3–6, doi:10.1029/2011GL046861, 2011. 18048

Huijnen, V., Williams, J., van Weele, M., van Noije, T., Krol, M., Dentener, F., Segers, A., Houweling, S., Peters, W., de Laat, J., Boersma, F., Bergamaschi, P., van Velthoven, P., Le Sager, P., Eskes, H., Alkemade, F., Scheele, R., Nédélec, P., and Pätz, H.-W.: The global chemistry transport model TM5: description and evaluation of the tropospheric chemistry version 3.0, Geosci. Model Dev., 3, 445–473, doi:10.5194/gmd-3-445-2010, 2010. 18038, 18057

Isaksen, I. S. A., Gauss, M., Myhre, G., Anthony, K. M. W., and Ruppel, C.: Strong atmospheric chemistry feedback to climate warming from Arctic methane emissions, Global Biogeochem. Cy., 25, GB2002, doi:10.1029/2010GB003845, 2011. 18042

Kinnison, D. E., Grant, K. E., Connell, P. S., Rotman, D. A., and Wuebbles, D. J.: The chemical and radiative effects of the Mount Pinatubo eruption, J. Geophys. Res., 99, 25705–25731, 1994. 18032

Lelieveld, J., Peters, W., Dentener, F. J., and Krol, M. C.: Stability of tropospheric hydroxyl chemistry, J. Geophys. Res., 107, 4715, doi:10.1029/2002JD002272, 2002. 18042

Lowe, D. C., Manning, M. R., Brailsford, G. W., and Bromley, A. M.: The 1991–1992 atmospheric methane anomaly: southern hemisphere 13C decrease and growth rate fluctuations, Geophys. Res. Lett., 24, 857–860, doi:10.1029/97GL00830, 1997. 18034

Madronich, S.: UV radiation in the natural and perturbed atmosphere, in: Environmental Effects of UV (Ultraviolet) Radiation, edited by: Tevini, M., 17–69, Lewis Publisher, Boca Raton, 1993. 18036

McCormick, M. P., Thomason, L. W., and Trepte, C. R.: Atmospheric effects of the Mt. Pinatubo eruption, Nature, 373, 399–404, 1995. 18032

Montzka, S. A., Dlugokencky, E. J., and Butler, J. H.: Non-CO_2 greenhouse gases and climate change, Nature, 476, 43–50, doi:10.1038/nature10322, 2011a. 18031

Montzka, S. A., Krol, M., Dlugokencky, E., Hall, B., Jockel, P., and Lelieveld, J.: Small Interannual Variability of Global Atmospheric Hydroxyl, Science, 331, 67–69, doi:10.1126/science.1197640, 2011b. 18031

Prather, M., Derwent, R., Ehhalt, D., Fraser, P., Sanhueza, E., and Zhou, X.: Other tracer gases and atmospheric chemistry, in: Climate Change 1995: The Science of Climate Change, Contribution of Working Group I to the Second Assessment Report of the Intergovernmental Panel on Climate Change, 73–126, Cambridge Univ. Press, 1996. 18042

Prather, M., Ehhalt, D., Dentener, F., Derwent, R., Dlugokencky, E., Holland, E., Isaksen, I. S. A., Katima, J., Kirchhoff, V., Matson, P., Midgley, P. M., and Wang, M.: Atmospheric chemistry and greenhouse gases, in: Climate Change 2001: The Scientific Basis, Contribution of

Working Group I to the Third Assessment Report of the Intergovernmental Panel on Climate Change, 239–288, Cambridge Univ. Press, New York, 2001. 18031, 18036

Prinn, R. G., Huang, J., Weiss, R. F., Cunnold, D. M., Fraser, P. J., Simmonds, P. G., McCulloch, A., Harth, C., Reimann, S., Salameh, P., O'Doherty, S., Wang, R. H. J., Porter, L. W., Miller, B. R., and Krummel, P. B.: Evidence for variability of atmospheric hydroxyl radicals over the past quarter century, Geophys. Res. Lett., 32, L07809, doi:10.1029/2004GL022228, 2005. 18031

Randel, J. W., Wu, F., Russell III, J., Waters, J., and Froidevaux, L.: Ozone and temperature changes in the stratosphere following the eruption of Mount Pinatubo, Geophys. Res. Lett., 100, 16753–16764, 1995. 18032, 18039

Ringeval, B., de Noblet-Ducoudré, N., Ciais, P., Bousquet, P., Prigent, C., Papa, F., and Rossow, W. B.: An attempt to quantify the impact of changes in wetland extent on methane emissions on the seasonal and interannual time scales, Global Biogeochem. Cy., 24, GB2003, doi:10.1029/2008GB003354, 2010. 18047

Russell, P. B., Livingston, J. M., Pueschel, R. F., Bauman, J. J., Pollack, J. B., Brooks, S. L., Hamill, P., Thomason, L. W., Stowe, L. L., Deshler, T., Dutton, E. G., and Bergstrom, R. W.: Global to microscale evolution of the Pinatubo volcanic aerosol derived from diverse measurements and analyses, J. Geophys. Res., 101, 18745–18763, 1996. 18032

Schauffler, S. M. and Daniel, J. S.: On the effects of stratospheric circulation changes on trace gas trends, J. Geophys. Res., 99, 25747–25754, 1994. 18034

Shindell, D. T., Faluvegi, G., Stevenson, D. S., Krol, M. C., Emmons, L. K., Lamarque, J.-F., Pétron, G., Dentener, F. J., Ellingsen, K., Schultz, M. G., Wild, O., Amann, M., Atherton, C. S., Bergmann, D. J., Bey, I., Butler, T., Cofala, J., Collins, W. J., Derwent, R. G., Doherty, R. M., Drevet, J., Eskes, H. J., Fiore, A. M., Gauss, M., Hauglustaine, D. A., Horowitz, L. W., Isaksen, I. S. A., Lawrence, M. G., Montanaro, V., Müller, J.-F., Pitari, G., Prather, M. J., Pyle, J. A., Rast, S., Rodriguez, J. M., Sanderson, M. G., Savage, N. H., Strahan, S. E., Sudo, K., Szopa, S., Unger, N., van Noije, T. P. C., and Zeng, G.: Multimodel simulations of carbon monoxide: comparison with observations and projected near-future changes, J. Geophys. Res., 111, D19306, doi:10.1029/2006JD007100, 2006. 18036, 18041

Soden, B. J., Wetherald, R. T., Stenchikov, G. L., and Robock, A.: Global cooling after the eruption of Mount Pinatubo: a test of climate feedback by water vapor, Science, 296, doi:10.1126/science.296.5568.727, 2002. 18033

Spahni, R., Wania, R., Neef, L., van Weele, M., Pison, I., Bousquet, P., Frankenberg, C., Foster, P. N., Joos, F., Prentice, I. C., and van Velthoven, P.: Constraining global methane emissions and uptake by ecosystems, Biogeosciences, 8, 1643–1665, doi:10.5194/bg-8-1643-2011, 2011. 18031, 18033, 18038, 18047

Stevenson, D. S., Dentener, F. J., Schultz, M. G., Ellingsen, K., van Noije, T. P. C., Wild, O., Zeng, G., Amann, M., Atherton, C. S., Bell, N., Bergmann, D. J., Bey, I., Butler, T., Cofala, J., Collins, W. J., Derwent, R. G., Doherty, R. M., Drevet, J., Eskes, H. J., Fiore, A. M., Gauss, M., Hauglustaine, D. A., Horowitz, L. W., Isaksen, I. S. A., Krol, M. C., Lamarque, J.-F., Lawrence, M. G., Montanaro, V., Müller, J.-F., Pitari, G., Prather, M. J., Pyle, J. A., Rast, S., Rodriguez, J. M., Sanderson, M. G., Savage, N. H., Shindell, D. T., Strahan, S. E., Sudo, K., and Szopa, S.: Multimodel ensemble simulations of present-day and near-future tropospheric ozone, J. Geophys. Res., 111, D08301, doi:10.1029/2005JD006338, 2006. 18041

Telford, P. J., Lathiere, J., Abraham, N. L., Archibald, A. T., Braesicke, P., Johnson, C. E., Morgenstern, O., O'Connor, F. M., Pike, R. C., Wild, O., Young, P. J., Hewitt, C. N., and Pyle, J.: Effects of climate-induced changes in isoprene emissions after the eruption of Mount Pinatubo, Atmos. Chem. Phys., 10, 7117–7125, doi:10.5194/acp-10-7117-2010, 2010. 18035, 18044, 18045

Thomason, L. W., Poole, L. R., and Deshler, T.: A global climatology of stratospheric aerosol surface area density as deduced from stratospheric aerosol and gas experiment II measurements: 1984–1994, J. Geophys. Res., 102, 8967–8976, 1997. 18032, 18039

Valentine, D. W., Holland, E. A., and Schimel, D. S.: Ecosystem and physiological controls over methane production in northern wetlands, J. Geophys. Res., 99, 1563–1571, doi:10.1029/93JD00391, 1994. 18047

Van Aardenne, J. A., Dentener, F. J., Olivier, J. G. J., Klein Goldewijk, C. G. M., and Lelieveld, J.: A high resolution dataset of historical anthropogenic trace gas emissions for the period 1890–1990, Global Biogeochem. Cy., 15, 909–928, 2001. 18038

Wang, J. S., Logan, J. A., Mcelroy, M. B., Duncan, B. N., Megretskaia, I. A., and Yantosca, R. M.: A 3-D model analysis of the slowdown and interannual variability in the methane growth rate from 1988 to 1997, Global Biogeochem. Cy., 18, GB3011, doi:10.1029/2003GB002180, 2004. 18034

Wang, Y. and Jacob, D. J.: Anthropogenic forcing on tropospheric ozone and OH since preindustrial times, J. Geophys. Res., 103, 31123–31135, 1998. 18041

Williams, J. E., Strunk, A., Huijnen, V., and van Weele, M.: The application of the modified band approach for the calculation of on-line photodissociation rate constants in TM5: implications for oxidative capacity, Geosci. Model Dev., 5, 15–35, doi:10.5194/gmd-5-15-2012, 2012. 18041

Wilton, D. J., Hewitt, C. N., and Beerling, D. J.: Simulated effects of changes in direct and diffuse radiation on canopy scale isoprene emissions from vegetation following volcanic eruptions, Atmos. Chem. Phys., 11, 11723–11731, doi:10.5194/acp-11-11723-2011, 2011. 18044

Table 1. Reactions included in the model. Reaction rates are the ones described in Huijnen et al. (2010), except from photolysis rates, which are computed using TUV.

Reactants	Products
$O_3 + h\nu$	$2 \times OH$
$NO_2 + h\nu$	$O_3 + NO$
$O_3 + NO$	NO_2
$O_3 + OH$	HO_2
$O_3 + HO_2$	OH
$HO_2 + HO_2$	
$HO_2 + OH$	
$HO_2 + NO$	$OH + NO_2$
$NO_2 + OH$	
$CO + OH$	HO_2
$CH_4 + OH$	$0.9 \times CO + RO_2$
$RH + OH$	$0.5 \times CO + RO_2$
$RO_2 + NO$	$NO_2 + y \times HO_2$
$RO_2 + HO_2$	
$RO_2 + RO_2$	

Table 2. Setup of the Pinatubo simulations.

Simulation name	Changes implemented in TUV	Changes implemented in the column chemistry model
SO_2	2.54 DU of SO_2 between 15 and 30 km altitude	Changes in photolysis frequencies from TUV
Aerosol	0.15 AOD due to Pinatubo between 15 and 30 km altitude	Changes in photolysis frequencies from TUV
Ozone	5 % ozone column decrease	Changes in photolysis frequencies from TUV
Temp Rates		Changed reaction rates due to temperature
H_2O		Changes in water vapour profile due to changed temperature profile
Methane Emis		Changes in methane emissions from wetlands due to temperature
Isoprene Emis		Changes in isoprene emissions due to temperature and PAR flux
Temp All		Changes in reaction rates, water vapour and emissions due to temperature

Table 3. Yearly emissions implemented in the model. Emission units are given in paranthesis.

Species (unit)	1890	1990
Methane ($Tg\,yr^{-1}$)	278	500
NO_x ($TgN\,yr^{-1}$)	21.3	45.3
CO ($Tg\,yr^{-1}$)	459	1081
NMVOC ($TgC\,yr^{-1}$)	707	800

Table 4. Comparison of the budgets for the global troposphere obtained with our one-dimensional model, with the ones of other models. Numbers in $Tg\,yr^{-1}$, unless otherwise specified.

	Stevenson et al. (2006), S1 scenario	Shindell et al. (2006)	Williams et al. (2012)	One-dimensional model
Ozone chemical production	5110 ± 606		4729	6167
Ozone chemical loss	4668 ± 727			4870
Ozone deposition	1003 ± 200		863	1323
Ozone stratospheric exchange	552 ± 168		274	27
Ozone burden (Tg)	344 ± 39		320	342
Ozone lifetime (days)	22.3 ± 2		23.4	20.2
OH ($molec\,cm^{-3}$)		11.3 ± 1.7		9.0
OH production from photolysis			1663	2097
OH chemical production			3522	3557
CO chemical production		1505 ± 236	1314	1656
CO burden (Tg)			322	386
CO lifetime (days)			48.3	51.4
CH_4 lifetime (yrs)	8.76 ± 1.32	9.7 ± 1.7	8.35	7.9

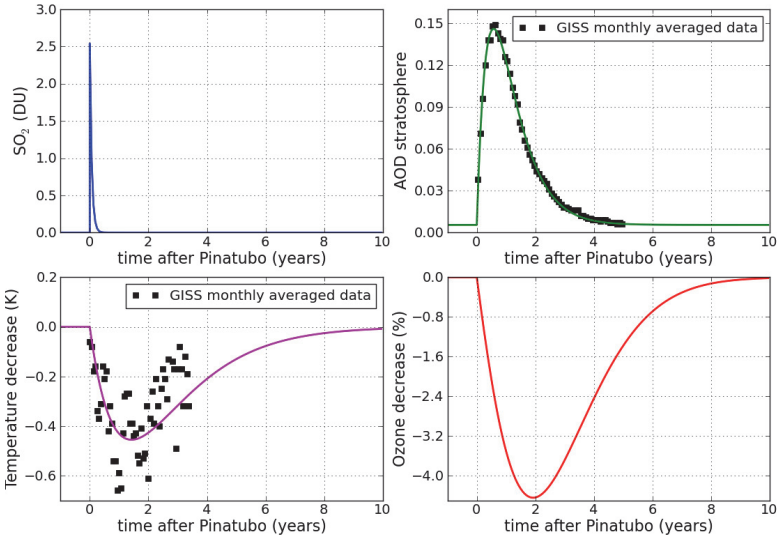

Fig. 1. Time evolution of the forcings, as implemented in the model. Squares represent monthly averaged GISS data.

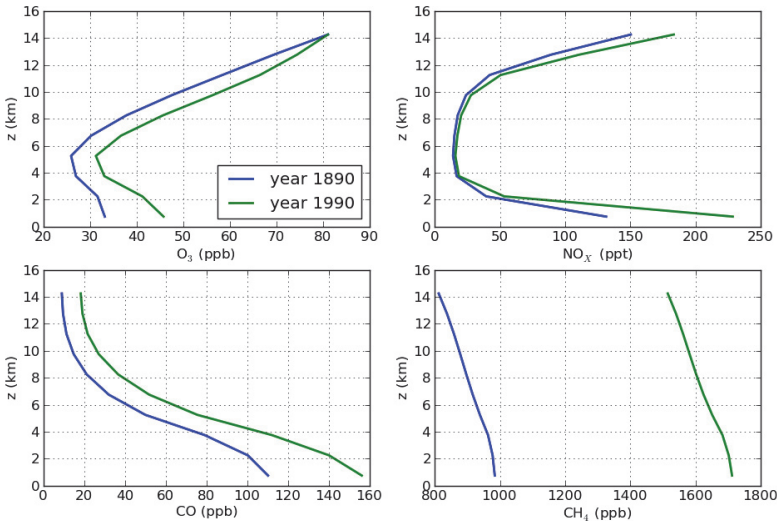

Fig. 2. Vertical profiles of ozone, NO_x, CO, and methane obtained with the one dimensional model for the years 1890 and 1990.

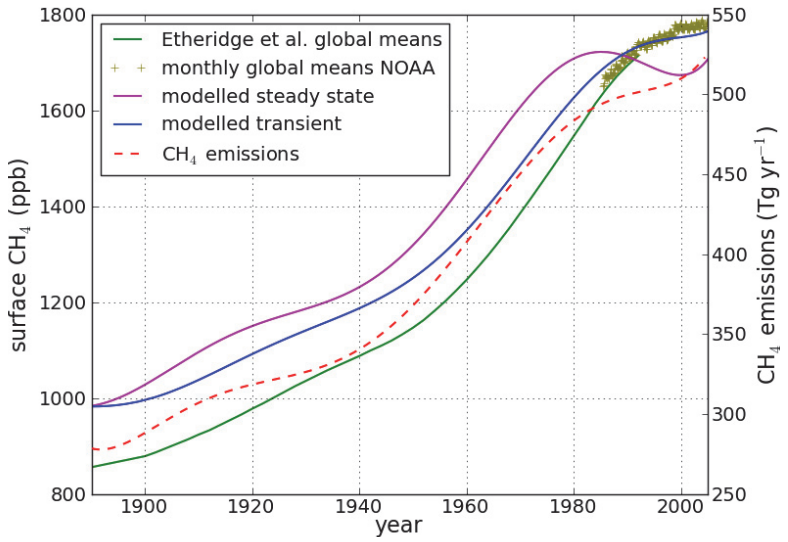

Fig. 3. Observed and modeled steady-state and transient evolution of methane surface concentrations between 1890 and 2005. Observation-based global means are calculated by Etheridge et al. (1998) based on ice-core data (green line), and more recent global means are calculated using measurements at South Pole and Alert NOAA stations (green crosses). Also methane emissions implemented in the model are shown (red dotted line, with scale on the right axis).

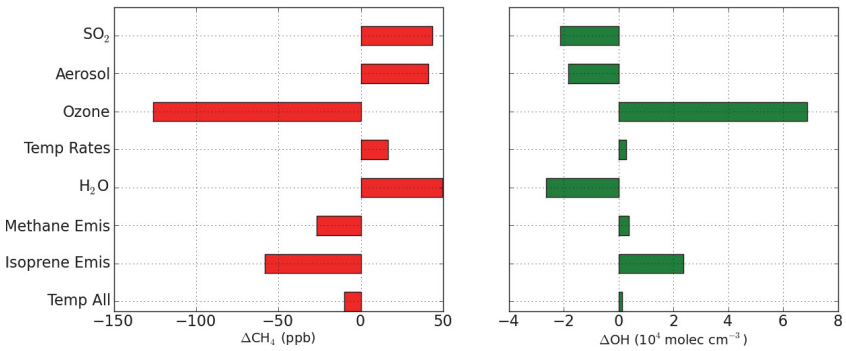

Fig. 4. Methane and OH steady-state changes due to Pinatubo forcings.

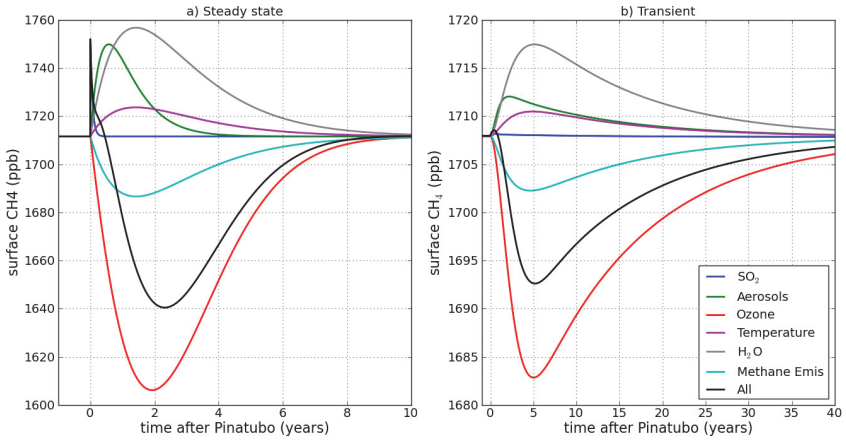

Fig. 5. Effect of the different Pinatubo forcings on surface methane **(a)** steady-state and **(b)** transient evolution.

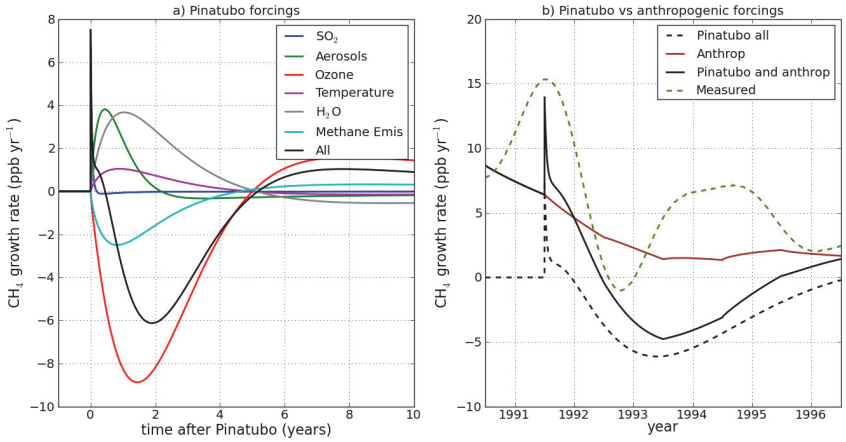

Fig. 6. Growth rate evolution after Pinatubo including **(a)** natural effects due to the eruption and **(b)** both natural effects due to the eruption and variation in anthropogenic emissions. Also shown in **(b)** is the global averaged growth rate obtained using the marine reference boundary matrix from GLOBALVIEW-CH4 (2009).